

# Conjugated Polymer Dots-on-Electrospun Fibers as a Fluorescent Nanofibrous Sensor for Nerve Gas Stimulant

Seonyoung Jo,<sup>†,‡</sup> Jongho Kim,<sup>†</sup> Jaeguk Noh,<sup>†</sup> Daigeun Kim,<sup>†</sup> Geunseok Jang,<sup>†</sup> Naeun Lee,<sup>§</sup> Eunji Lee,<sup>§</sup> and Taek Seung Lee<sup>\*,†</sup>

<sup>†</sup>Organic and Optoelectronic Materials Laboratory, Department of Advanced Organic Materials and Textile System Engineering, Chungnam National University, Daejeon 305-764, Korea

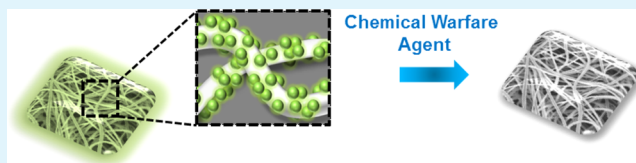
<sup>‡</sup>Dongjin Semichem Co., Electronic Materials Business Division, Jageundollae-gil 35, Yanggam-myeon, Hwaseong-si, Gyeonggi-do 445-935, Korea

<sup>§</sup>Graduate School of Analytical Science and Technology, Chungnam National University, Daejeon 305-764, Korea

## S Supporting Information

**ABSTRACT:** A novel chemical warfare agent sensor based on conjugated polymer dots (CPdots) immobilized on the surface of poly(vinyl alcohol) (PVA)–silica nanofibers was prepared with a dots-on-fibers (DoF) hybrid nanostructure via simple electrospinning and subsequent immobilization processes. We synthesized a polyquinoxaline (PQ)-based CP as a highly emissive sensing probe and employed PVA–silica as a host polymer for the electrospun fibers. It was demonstrated that the CPdots and amine-functionalized electrospun PVA–silica nanofibers interacted via an electrostatic interaction, which was stable under prolonged mechanical force. Because the CPdots were located on the surface of the nanofibers, the highly emissive properties of the CPdots could be maintained and even enhanced, leading to a sensitive turn-off detection protocol for chemical warfare agents. The prepared fluorescent DoF hybrid was quenched in the presence of a chemical warfare agent simulant, due to the electron transfer between the quinoxaline group in the polymer and the organophosphorous simulant. The detection time was almost instantaneous, and a very low limit of detection was observed ( $\sim 1.25 \times 10^{-6}$  M) with selectivity over other organophosphorous compounds. The DoF hybrid nanomaterial can be developed as a rapid, practical, portable, and stable chemical warfare agent-detecting system and, moreover, can find further applications in other sensing systems simply by changing the probe dots immobilized on the surface of nanofibers.

**KEYWORDS:** conjugated polymer dots, PVA–silica nanofibers, hybrid nanostructure, chemical warfare agent, nanofiber sensors



## 1. INTRODUCTION

Fluorescent conjugated polymers serving as active components in organic light-emitting diodes, photoconductors, and sensors have constituted an attractive research field during recent decades.<sup>1–3</sup> In particular, the fluorescence intensity of conjugated polymer-based fluorescent sensors can be altered upon binding to an analyte, because of the electron transfer and energy transfer between the polymer and a quenching species.<sup>4–6</sup> One of the most interesting classes of conjugated polymer-comprising units, quinoxaline is a typical electron-deficient group, due to the strong electronegativity of the two nitrogen atoms. Many conjugated polymers containing electron donor–acceptor groups in the main chain have been designed using quinoxaline or its derivatives as electron-accepting moieties.<sup>7–9</sup>

To overcome the need for complicated synthetic works to introduce water solubility into hydrophobic conjugated polymers, simple methods of fabricating nanoparticles from hydrophobic CPs have been widely explored.<sup>9–13</sup> The resultant fluorescent CPdots have many advantages, including ease of fabrication, high fluorescence, high biocompatibility, and

excellent photostability.<sup>14–17</sup> These CPdots have, therefore, motivated numerous studies for lighting and targeted cellular imaging purposes, in which almost investigations were focused on biologically related fields.<sup>18–22</sup>

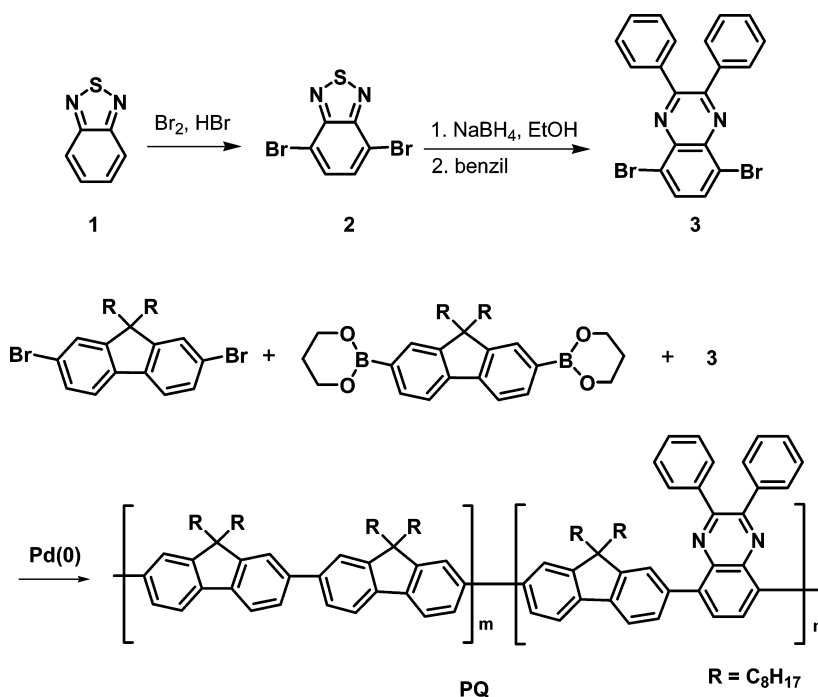
Hybrid nanostructures or multiple nanosystems have attracted a great deal of attention, because of the possible incorporation of multiple functions into a single unit.<sup>23–25</sup> Because more than one type of nanostructure can be incorporated into a single system, multiple functions can be potentially attained. These hybrid structures are of great interest in a variety of applications, because of their potential usefulness in parallel applications including biomedical and sensory fields.<sup>26,27</sup> Among the various hybrid materials, a great deal of attention has been focused on the assembly of functional inorganic and organic hybrid nanostructures, because the advantages of both organic and inorganic properties can be effectively combined.<sup>28–30</sup>

**Received:** October 18, 2014

**Accepted:** November 28, 2014

**Published:** November 28, 2014

Scheme 1. Synthesis of Monomer and PQ



Considering these conditions, electrospinning can be a potential preparative candidate for hybrid nanosystems because it provides an efficient and versatile technique to fabricate fibrous nanowebs with a large surface area and porous nanostructure suitable for the adsorption of other materials, which is useful in sensing applications.<sup>31,32</sup> Electrospun nanofibers have been applied to fluorescent sensors for metal ions, gas, and pH via the incorporation of recognition probes on their surface or within them.<sup>33–35</sup> Moreover, the integration of fluorescent materials into electrospun nanofibers has been conducted for the fabrication of multicompartiment nanofibers<sup>36–38</sup> to be applied in efficient fluorescent sensory hybrid materials.<sup>39,40</sup> Moreover, nanofibers containing various types of silica materials have been developed for the formation of organic and inorganic hybrid materials.<sup>41,42</sup>

Many difficulties in preparing multicompartimental hybrid nanofibers by electrospinning have been reported, resulting from the poor dispersion of the additives, leading to needle clogging and a negative effect on their spinnability.<sup>43,44</sup> In this study, therefore, CPdots were introduced on the surface of the nanofibers after the spinning process. It has been proved that, and as can be easily imagined, the fluorescent properties of multicompartimental nanofibers, in which CPdots are assembled on the surface, are superior to those in which CPdots are embedded inside the nanofibers, in terms of their quantum yields.<sup>45,46</sup> Because of their high aspect ratios and large specific surface areas, two-dimensional (2D) fibrous nanoweb materials afford a high adsorption capacity. Their high adsorption capacity makes it possible to apply them to facile conjugation with organic particles on their surfaces.

Herein, we explored the fabrication of organic–inorganic hybrids, demonstrating a novel DoF conjugated system, where a number of CPdots are located in a random fashion (but not superposed) over the surface of the nanofibers. Interestingly and importantly, the CPdots and nanofibers assembled in aqueous solution to afford a DoF hybrid system that retained

the emission properties of the pristine CPdots with a much higher quantum yield.

Moreover, using the DoF hybrid nanomaterials, we attempted to extend the application fields of CPdots to the detection of chemical warfare agents, in which polyquinoxaline-based CPdots were used as the probe molecules and electrospun nanofibers as the supporting matrix. It is known that chemical warfare agents, such as Sarin, Soman, and Tabun, are highly reactive, volatile, and toxic organophosphorous compounds, whose action arises from the disruption of the message-transferring process of nerves to organs. The inhalation of chemical warfare agents can lead to organ failure and eventual death within minutes.<sup>47,48</sup> Thus, extensive analytical methods for the detection of organophosphorous nerve agents have been developed using fluorogenic and chromogenic probes,<sup>49–53</sup> including conjugated polymer-based sensors as sensing elements.<sup>9,54</sup> However, most techniques are based on the use in a solution system, which might hinder the practical applications.

We envisioned the use of DoF in a fiber-based, fluorescent sensing protocol for chemical warfare agents. To our knowledge, there have been no reports on a reliable and stable fabrication method of DoF with a well-defined nanostructure and on a stable and practical sensing platform for chemical warfare agents. It should be emphasized that this approach encounters fundamental challenges in materials chemistry. The assembly of CPdots on the surface of nanofibers opens up a new horizon for achieving three-dimensional (3D) architectures using zero-dimensional (0D) dots and 2D nanowebs as building blocks.

## 2. RESULTS AND DISCUSSION

**Synthesis and Characterization.** Scheme 1 shows the synthetic routes for monomer **3** and **PQ**. Commercially available 2,1,3-benzothiadiazole (**1**) was used for the synthesis of the dibromoquinoxaline monomer **3**. 4,7-Dibromo-2,1,3-benzothiadiazole (**2**) was synthesized via the bromination of **1**. **2**

was easily reduced to 3,6-dibromobenzene-1,2-diamine in the presence of sodium borohydride, and its subsequent reaction with benzil provided 5,8-dibromo-2,3-diphenylquinoxaline (**3**) according to previously published methods.<sup>55</sup> The polymer **PQ** was synthesized via the palladium-catalyzed Suzuki-coupling reaction. **PQ** exhibited good solubility in common organic solvents, including tetrahydrofuran (THF), chloroform, and toluene. The chemical structure of **PQ** was confirmed by <sup>1</sup>H NMR, <sup>13</sup>C NMR, FT-IR, and element analysis (EA). According to the EA data, the molecular composition (*m:n*) of **PQ** was found to be 0.82:0.18 as a mole fraction. The number-average molecular weight (*M<sub>n</sub>*) and weight-average molecular weight (*M<sub>w</sub>*) were found to be 6920 and 13760, respectively, as determined with gel permeation chromatography using polystyrene as the standard and chloroform as the eluent.

**Optical Properties.** The absorption and fluorescence emission spectra of **PQ** in chloroform solution and in the form of a solid film are shown in Figure 1. The absorption

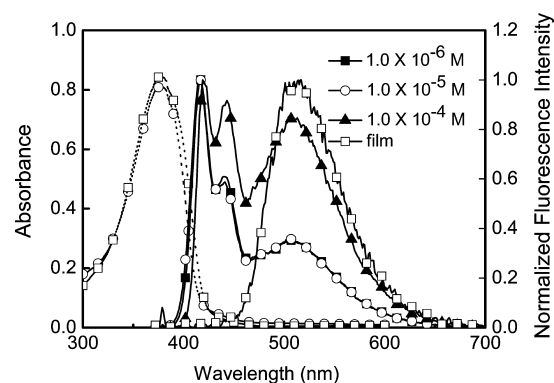


**Figure 1.** Absorption (dotted) and normalized fluorescence spectra (solid) of **PQ** in chloroform solution and in the film. For absorption spectra, empty circles correspond to the solution ( $1.0 \times 10^{-5}$  M) and empty squares to the film.

bands of **PQ** both in solution and in the form of a solid film were observed at 377 nm, and were attributed to the  $\pi$ - $\pi^*$  transition of the conjugated segments. In contrast to its similar absorption in solution and in the solid state, the emission of **PQ** varied depending upon its concentrations and phase. Interestingly, the fluorescence emission of **PQ** showed a dominant short wavelength emission in the range from 400 to 450 nm in dilute solution ( $1.0 \times 10^{-6}$  to  $1.0 \times 10^{-5}$  M). However, the intensity of the longer wavelength emission at 510 nm was enhanced in a more concentrated solution of **PQ** and, finally, only the longer wavelength emission was observed in the film state. The long-wavelength emission was mainly afforded by the quinoxaline units, whose intensity was enhanced by the energy transfer from the fluorene units in the aggregated state.<sup>56,57</sup> The concentration dependency of the emission changes of **PQ** could be easily observed with the naked eye under UV illumination, as shown in Figure S1 (Supporting Information). This concentration-dependent or aggregation-induced emission change was attributed to the intermolecular exciton migration, which was triggered by aggregation between the polymer chains, as found in the conjugated polymers containing both electron donor (fluorene) and acceptor (quinoxaline) groups in the same backbone.<sup>58-62</sup>

**Preparation of CPdots from **PQ**.** CPdots were fabricated through a reprecipitation method from **PQ**. Briefly, a THF solution of **PQ** was injected into water under continuous

sonication. After the removal of THF, the solution was filtered by a syringe filter. The SEM image of the CPdots showed that they were spherically shaped (Figure 2a) and the average diameter of the CPdots was determined by dynamic light scattering (DLS), indicating that the hydrodynamic diameter was  $66.28 \pm 1.84$  nm (Figure S2, Supporting Information). The zeta-potential of the CPdots was measured to be  $-38.6 \pm 0.7$  mV in a neutral aqueous solution, resulting in their dispersion remaining clear and stable for 2 weeks without any sign of aggregation.

As shown in Figure 3, as in the case of the solution of **PQ**, the CPdots from **PQ** in aqueous solution exhibited an absorption at 380 nm and maximum emission at 501 nm with an emission tail extending to 600 nm. The relative quantum yield (QY) of the aqueous CPdot solution was measured to be 13% using rhodamine B as the standard, while the absolute QY of the solid CPdots was found to be 12% using an integrating sphere (Table S1, Supporting Information).

**Preparation and Characterization of DoF.** Meanwhile, for the fabrication of the organic-inorganic hybrid nanofibers, a mixture of PVA and tetraethyl orthosilicate (TEOS) was prepared, incubated in the presence of acid, and, finally, electrospun into a nanoweb. Because the nanofibers made from pure PVA were soluble in water and lost their dimension in aqueous solution, PVA was cross-linked with TEOS using an acid-catalyzed sol-gel process to obtain PVA-silica hybrid nanofibers.<sup>63</sup> To confirm the incorporation of silica into PVA matrix, the FT-IR, TGA, and XPS spectra of the PVA-silica nanofibers were compared with those of pure PVA. As shown in Figure S3 (Supporting Information), the PVA nanofibers showed the characteristic bands of the hydroxyl and aliphatic hydrocarbon groups at around 3300 and 2900  $\text{cm}^{-1}$ , respectively. The band intensity of the hydroxyl group in the PVA-silica nanofibers was decreased due to the reduction of the number of hydroxyl groups, because of their reaction with TEOS. In this experiment, PVA with a degree of saponification of 88% was used, resulting in the appearance of the characteristic band of the carbonyl group at around 1700  $\text{cm}^{-1}$ , which can be frequently observed in the incompletely hydrolyzed (saponified) PVA from poly(vinyl acetate), while the completely hydrolyzed PVA does not show the characteristic C=O band. The characteristic bands of Si-O-Si in the PVA-silica nanofibers are observed between 1000 and 1100  $\text{cm}^{-1}$ . The TGA thermograms of the nanofibers indicate that about 60 wt % of inorganic components was incorporated into the nanofibers (Figure S4, Supporting Information). The weight loss in the PVA nanofibers occurred at 350–500 °C because of the cleavage of the C-C bond. The XPS spectra confirmed the successful synthesis of organic-inorganic hybrid nanofibers, as shown in Figure S5a and b (Supporting Information). On the basis of these findings, it can be concluded that water-insoluble, thermally stable, organic-inorganic hybrid nanofibers were successfully fabricated by electrospinning.

Finally, the surface of the PVA-silica nanofibers was modified to obtain the amine functionality using (3-aminopropyl)triethoxysilane (APTES) via a simple after-treatment method.<sup>64</sup> XPS analysis of the APTES-treated PVA-silica nanofibers showed the presence of nitrogen atoms, which were incorporated by the APTES modification (Figure S5c, Supporting Information). The SEM images of the PVA nanofibers and APTES-treated PVA-silica nanofibers can be seen in parts b and c of Figure 2, respectively. After the

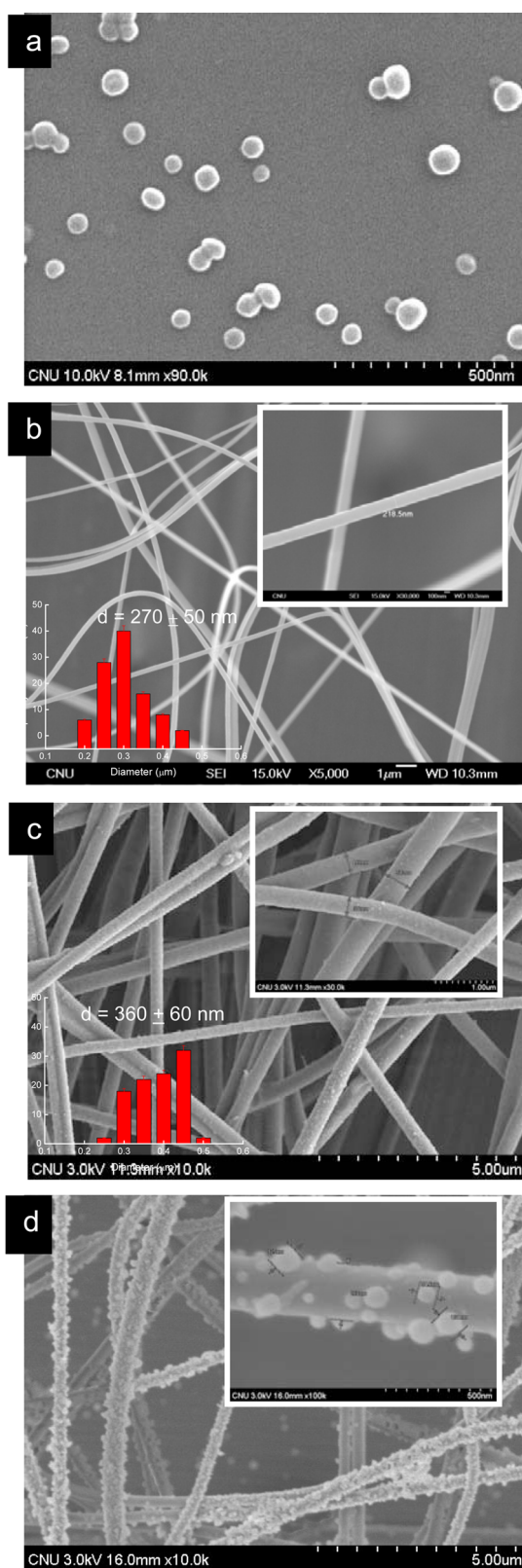


**Figure 2.** SEM images of the CPdots from PQ (a), electrospun PVA-silica nanofibers (b), nanofibers after treatment with APTES (c), and subsequent incubation with CPdots (d). Inset: High-magnification SEM images of nanofibers. The number above each histogram represents the average diameter of nanofibers estimated from more than 100 nanofibers.

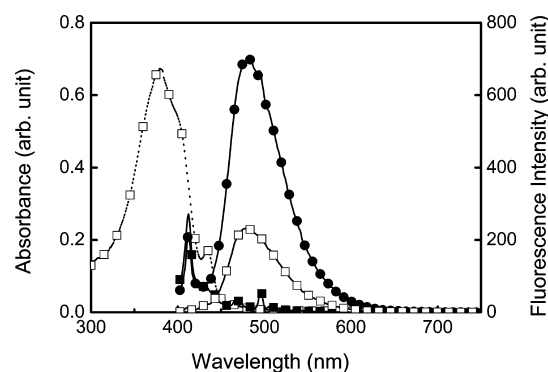


**Figure 3.** Absorption (dotted) and fluorescence spectra (solid) of CPdots from PQ (□), PVA-silica nanofibers (■), and DoF (●). [CPdots] =  $8.3 \times 10^{-2}$  mg/mL. The fabrication method for DoF is described in the Experimental Section.

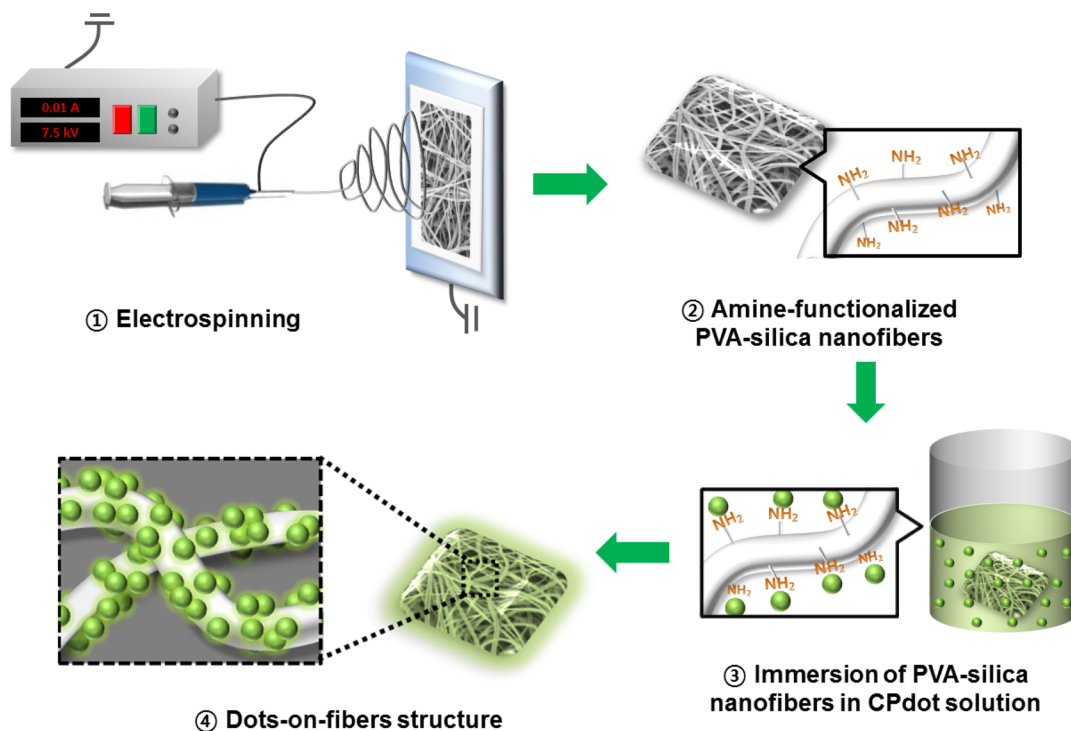
APTES treatment, the surface of the nanofibers was observed to be rougher and their diameter increased (PVA-silica nanofibers before APTES treatment,  $270 \pm 50$  nm; after APTES treatment,  $360 \pm 90$  nm).

A schematic illustration of the synthetic process for the fluorescent DoF hybrid nanostructure is demonstrated in Scheme 2. The fabrication process for the DoF structure was composed of four steps. First, PVA-silica organic-inorganic hybrid nanofibers were obtained via electrospinning for their water insolubility and chemical and thermal stability. Second, the nanofibers were treated with APTES and subjected to subsequent baking at  $100^\circ\text{C}$  to introduce amine groups on their surface. Third, the amine-modified PVA-silica nanofibers were immersed in aqueous CPdot solution. Finally, the DoF nanostructure was successfully obtained via the electrostatic interaction between the positively charged nanofibers and negatively charged CPdots.

The distribution of the CPdots on the surface of the hybrid nanofibers was observed using SEM (Figure 2d). The CPdots were successfully attached on the surface of the nanofibers, as confirmed by the strong fluorescence in the fluorescence microscopic images (Figure S6, Supporting Information). The DoF assembly was accomplished by the electrostatic attraction between the positively charged amine-modified PVA-silica nanofibers and negatively charged CPdots. The SEM images of the two kinds of nanofibers, untreated and treated with APTES followed by the immobilization of the CPdots, were compared (Figure S7, Supporting Information). The CPdots were attached only to the amine-functionalized PVA-silica nanofibers, while the PVA-silica nanofibers that were not treated with APTES did not show any assembled CPdots on their surface. This reveals that the assembly took place via electrostatic interaction and, therefore, the amine functionality of the matrix nanofibers was indispensable to immobilize the CPdots, similar to our previous results.<sup>64</sup> The emission spectrum of the DoF is almost the same as that of the CPdots with an emission maximum at around 500 nm (Figure 3).

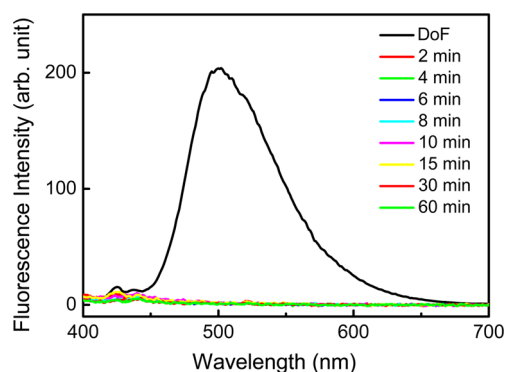
To gain insight into the electrostatic attraction between the PVA-silica nanofibers and CPdots, the pH of the aqueous solutions in which the immobilization occurred was manipulated. As shown in Figure S8a (Supporting Information), the zeta-potential of the CPdots was remarkably influenced by the pH of the aqueous solution, showing a decrease with increasing pH. At low pH, the CPdots have less negative charge and, thereby, should have less electrostatic interaction with the

**Scheme 2. Schematic Illustration for Fabrication of DoF Structure:** ① Fabrication of PVA–Silica Nanofibers via Electrospinning with a Mixed Solution of PVA and TEOS; ② Treatment of the Nanofibers with APTES to Give Amine Functionality; ③ Immersion of the Amine-Functionalized PVA–Silica Nanofibers in CPdot Solution to Immobilize CPdots on the Surface of the Nanofibers; ④ Formation of Fluorescent DoF Nano-hybrid Structure



positively charged amine-modified PVA–silica fibers. Parts b and c of Figure S8 (Supporting Information) show the SEM images of the DoF structures obtained at low pH values of 3.2 and 5.1, respectively, indicating that the immobilization was not successfully conducted. However, after immobilization at higher pH values ranging from 6.8 to 11.8, the CPdots were densely introduced onto the surface of the nanofibers (Figure S8d–f, Supporting Information). This indicates that interaction between the amine-functionalized nanofibers and CPdots was accomplished electrostatically. The successful modification of the CPdots on the surface of the nanofibers was confirmed by investigating the binding stability. It was found that the DoF was stable enough to withstand continuous centrifugation in an aqueous medium for up to 60 min by measuring the fluorescence spectra of the supernatants afterward (Figure 4). The fluorescence of the supernatants was very weak, indicating the strong binding of the CPdots to the nanofiber matrix.

The quantum yield (QY) of PQ can be as high as 37% (relative to rhodamine B) in chloroform solution (Table 1). In contrast, a lower QY (5–12%, absolute values from integrating sphere) of PQ was observed in its solid states (film, solid CPdots, PQ-blended in PMMA nanofibers, and CPdots-encapsulated within nanofibers) compared to that of its chloroform solution (37%). Interestingly, the highest absolute QY value of 48% was observed in the DoF structure prepared through the simple immobilization of CPdots onto nanofibers (immobilized hybrid), while only a QY of 20% was observed in the CPdots encapsulated within nanofibers (encapsulated hybrid). It has been reported that the chemically bonded immobilization of luminescent substances on a rigid support leads to an increase in the emission intensity, QY, and lifetime, which is attributed to the complete prevention of molecular







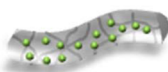


**Figure 4.** Fluorescence spectra of DoF and supernatants from DoF-immersed solutions after various centrifugation times at 14 000 rpm.

movement.<sup>65,66</sup> Meanwhile, the CPdots encapsulated within the PVA–silica nanofibers exhibited a much higher QY (20%), as compared to those encapsulated within the pure PVA nanofibers (5%), presumably due to the agglomeration and possible phase separation in the composite materials.<sup>67</sup> The absolute QY of 48% is a remarkably high value that can be obtained using CPdots from PQ, as compared with the best relative QY of conjugated polymer nanoparticles (65%, quinine sulfate as a reference).<sup>30</sup> The nonsuperimposed distribution of the negative CPdots on the surface of the PVA–silica nanofibers was mainly due to the electrostatic repulsion between them, leading to their positioning with a suitable distance for the good preservation of their original fluorescence properties.

**Detection Test of DCP Using DoF.** To further demonstrate the ability of the developed DoF structure for

Table 1. Quantum Yields of PQ in Various States

	Samples	QYs (%) <sup>a)</sup>
	PQ film	5
	CPdots from PQ (solid)	12
	PQ in chloroform solution	37 <sup>b)</sup>
	PQ blended in PMMA nanofibers	6
	CPdots encapsulated in PVA nanofibers	5
	CPdots encapsulated in PVA-silica nanofibers	20
	Dots-on-Fibers (CPdots immobilized on PVA-silica nanofibers)	48

<sup>a)</sup>QYs were determined with a calibrated integrating sphere (excitation source 325 nm laser). <sup>b)</sup>Relative to rhodamine B.

sensing applications, the detection of a chemical warfare agent simulant was attempted. Because real organophosphorous compounds are highly toxic, a mimicking compound such as diethyl chlorophosphate (DCP) is frequently used, which has similar reactivity but far less toxicity. The fluorescence response of DoF to trace DCP was determined in the concentration range 0–1.8 mM in ethanolic solution of DCP. Obvious fluorescence quenching at 501 nm was observed instantaneously upon exposure to DCP, as shown in Figure 5a. It has been reported that the emission quenching of polyquinoxaline-containing polymers results from the specific interaction between the quinoxaline groups and chemical warfare agents through the nucleophilic attack of quinoxaline on the electrophilic target (DCP).<sup>9</sup> The sensitivity of this system with various concentrations of DCP was investigated, as shown in Figure 5b. It was found that the detection limit of DoF toward DCP was  $1.25 \times 10^{-6}$  M (based on the  $3\sigma/\text{slope}$ , where  $\sigma$  is the standard deviation of four independent measurements), which is comparable to those from other techniques.<sup>51,52</sup> Moreover, the limit of detection was more enhanced than that from our previous sensing system, which was composed of a paper-based sensor protocol.<sup>9</sup> It is regarded that this high sensitivity resulted from the high QY of DoF which, in turn, made the fluorescence easily noticeable even at lower concentrations of the quencher, DCP.

The quenching response of the DoF can be explained through the measurement of the Stern–Volmer constant ( $K_{SV}$ ) described in the equation  $I_0/I = 1 + K_{SV}[Q]$ , where  $I_0$  and  $I$  are the fluorescence intensities in the absence and presence of

DCP, respectively, and  $[Q]$  corresponds to the concentration of the added quencher, DCP.<sup>68</sup> This equation provides a quantitative correlation between the changes in the fluorescence intensity of the DoF, which is dependent on the concentration of DCP. The presence of DCP quenched the fluorescence of the DoF with a linear relationship in the concentration range 0–1.8 mM (correlation coefficient of 0.990). The linear relationship between the concentration of DCP and  $I_0/I$  enabled us to obtain the  $K_{SV}$  value of DoF from the slope of the plot (Figure 5b), and it was found to be  $3.88 \times 10^2 \text{ M}^{-1}$ . It is presumed that the relatively low  $K_{SV}$  compared to the cases of other conjugated polymers stems from the fact that this sensing system was based on the solid-state quenching system, while most other systems were usually carried out in their solutions.

It is important to rapidly and selectively detect chemical warfare agent simulants for practical applications in the field. In order to investigate the selective detection of DCP, a class of phosphorus compounds, including dimethyl methylphosphonate (DMMP), triethylphosphate (TEP), and tributylphosphate (TBP), were exposed to the DoF using a similar method to that adopted for DCP. It appears that the relative fluorescence intensity of DoF was not influenced by the addition of DMMP, TEP, or TBP, presumably due to their lack of reactivity toward the quinoxaline group in the polymer (Figure 6 and Figure S9, Supporting Information). Table 2 summarizes the  $K_{SV}$  values of DoF toward organophosphorous compounds, in which the DoF had a considerably high selectivity to DCP. It can be concluded that, with the aid of

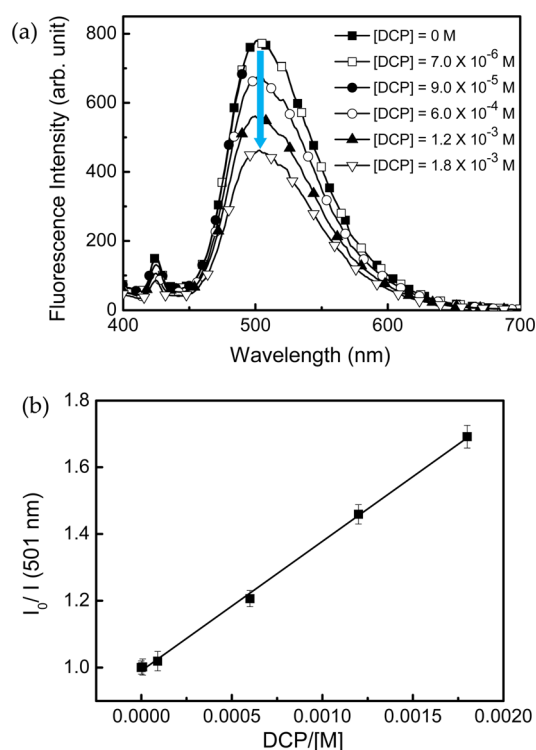


**Figure 5.** (a) Changes in fluorescence spectra of DoF upon exposure to DCP and (b) Stern–Volmer plot of DoF in response to DCP.  $I_0$  and  $I$  correspond to the emission intensity at 501 nm in the absence and presence of DCP, respectively.

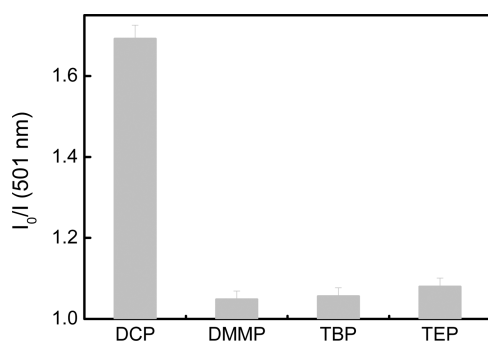


**Figure 6.** Relative fluorescence intensity ( $I_0/I$ ) of DoF.  $I_0$  and  $I$  correspond to the emission intensity at 501 nm in the absence and presence of organophosphorous compounds ( $1.8 \times 10^{-3}$  M), respectively.

**Table 2.** Stern–Volmer Constants of DoF in the Presence of Organophosphorous Compounds

	DCP	DMMP	TBP	TEP
$K_{SV}$ ( $M^{-1}$ )	388	23	29	44

the high specific surface area of the 2D nanofiber webs, a larger amount of CPdots could be introduced and, therefore, the resultant 3D DoF became more sensitive to small changes in external stimuli compared to the bulk materials. We, therefore, took advantage of the nanosized effects of nanofibers for the detection of DCP.

### 3. CONCLUSIONS

We synthesized a quinoxaline-based fluorescent conjugated polymer and fabricated a novel nanohybrid material with 3D

DoF structure by means of the attractive interaction between the conjugated polymer nanoparticles and electrospun PVA–silica nanofibers. Through investigating various techniques, the DoF was assembled via electrostatic attraction. The large enhancement of the fluorescence intensity of the DoF was confirmed by measuring the QY, which encouraged their possible use as a highly sensitive composite material for sensory applications. The DoF hybrid nanostructure showed high selectivity to DCP over other organophosphorous compounds with respect to its efficient fluorescence quenching. We anticipate that DoF will be useful for the fluorogenic detection of chemical warfare agents in a practical, rapid, and convenient way through stably immobilized CPdots on a suitable matrix such as fibers and papers.

### 4. EXPERIMENTAL SECTION

**Materials and Reagents.** All chemicals were purchased from commercial suppliers and used as received without further purification. 2,1,3-Benzothiadiazole, 9,9-dioctylfluorene-2,7-diboronic acid bis(1,3-propanediol) ester, 9,9-dioctyl-2,7-dibromofluorene, tetrakis-(triphenylphosphine)palladium, DCP, DMMP, TEP, and TBP were purchased from Sigma-Aldrich. Hydrochloric acid (37%), PVA ( $M_w$  205000 Da, 88% hydrolyzed), and TEOS were purchased from Samchun Chemicals and used as received. APTES was supplied by Tokyo Chemical Industry.

**Characterization.** The NMR spectra were collected from a Bruker DRX-300 spectrometer with tetramethylsilane as the internal standard (Korea Basic Science Institute). The IR spectra were recorded on a Bruker FT-IR spectrometer. Elemental analysis was performed on an Elemental Analyzer EA 1108 (Fisons Instruments). The UV–vis absorption spectra were recorded on a PerkinElmer Lambda 35 spectrometer. The photoluminescence spectra were obtained from a Varian Cary Eclipse fluorescence spectrophotometer equipped with a xenon flash lamp excitation source. The zeta-potentials and size distributions were measured using dynamic light scattering (DLS, Zetasizer Nano ZS, Malvern). X-ray photoelectron spectroscopy (XPS) analysis was carried out on a Thermo Scientific MultiLab 2000. The fluorescence microscopy images were taken using an Olympus BX53. Scanning electron microscopy was performed using a JSM-7000F, JEOL FESEM instrument. The photoluminescence quantum yields were measured in an integrating sphere (Labsphere Co.) equipped with a He–Cd laser (CW, 325 nm) as an excitation source, a monochromator (Acton Research Co.), and a photomultiplier tube (Hamamatsu Photonics K. K. Co.) used for detection. To avoid the degradation of the samples by laser excitation, the integrating spheres were kept in a nitrogen gas environment.

**Synthesis of 4,7-Dibromo-2,1,3-benzothiadiazole (2).** 2,1,3-Benzothiadiazole (2.0 g, 14.69 mmol) was suspended in HBr (30 mL, 48% in  $H_2O$ ) in a three-neck flask equipped with a reflux condenser and a dropping funnel containing a mixture of bromine (1.93 mL) and HBr (25 mL). After the addition of a few drops of the mixture, the solution color turned to orange and an orange colored precipitate appeared. Afterward, the mixture was stirred under reflux for 6 h, forming a yellow precipitate. After cooling the reaction mixture, the excess bromine was evaporated under a mild stream of air. The suspension was isolated by vacuum-filtration and washed with a large amount of water. The residue was then recrystallized from boiling methanol to give yellow crystals of **2** (yield 2.87 g, 66%).  $^1H$  NMR (300 MHz,  $CDCl_3$ ):  $\delta$  = 7.74 (s, 2H) ppm.

**Synthesis of 5,8-Dibromo-2,3-diphenylquinoxaline (3).** 3,6-Dibromobenzene-1,2-diamine (0.8 g, 3 mmol), which was obtained from the reduction of **2** (1.03 g, 3.5 mmol), was dissolved in acetic acid (30 mL), and then, the mixture was refluxed. Benzil (0.63 g, 3 mmol) was added into the mixture portion-wise. After 18 h, the reaction mixture was precipitated in ethanol and isolated by filtration. The precipitates were purified by recrystallization in ethanol. Further purification was carried out with column chromatography (ethyl acetate and *n*-hexane). After drying in a vacuum oven, the resulting

yellow solid was collected (yield 0.50 g, 37%).  $^1\text{H}$  NMR (300 MHz,  $\text{CDCl}_3$ ):  $\delta$  = 7.73 (s, 2H), 7.66–7.64 (t, 4H), 7.57–7.54 (m, 6H) ppm. Anal. Calcd (%) for  $\text{C}_{20}\text{H}_{12}\text{Br}_2\text{N}_2$ : C, 54.58; H, 2.75; N, 6.36; Found: C, 54.74; H, 2.73; N, 6.47.

**Synthesis of PQ.** A round-bottomed flask was charged with **3** (40 mg, 0.041 mmol), 9,9-dioctyl-2,7-dibromofluorene (0.20 g, 0.369 mmol), and 9,9-dioctyl fluorene-2,7-diboronic acid bis(1,3-propanediol) ester (0.27 g, 0.492 mmol) and then purged with nitrogen gas. The flask was degassed several times to ensure the complete removal of oxygen. After degassing, toluene (5 mL),  $\text{Pd}(\text{PPh}_3)_4$  (0.024 g, 0.021 mmol), 2 M aqueous potassium carbonate solution (3 mL), and water (2 mL) were added to the reaction mixture, which was refluxed for 48 h. After cooling, the mixture was poured into excess methanol and the precipitate was washed with acetone, methanol, and water, affording a green powder (yield 0.41 g, 58%).  $^1\text{H}$  NMR (300 MHz,  $\text{CDCl}_3$ ):  $\delta$  = 7.78–7.64 (m), 2.13 (t), 1.27–0.81 ppm (m).  $^{13}\text{C}$  NMR ( $\text{CDCl}_3$ ):  $\delta$  = 151.83, 126.17, 119.97, 55.35, 40.38, 31.80, 30.93, 30.05, 29.23, 23.93, 22.61, 14.07 ppm. FT-IR ( $\text{cm}^{-1}$ ): 2852 ( $\text{sp}^3$  C–H), 1610 (C=C), 1452 (aryl C=C). Anal. Calcd for  $\text{C}_{56.4}\text{H}_{79}\text{N}_{0.36}$ : C, 89.2; H, 10.5; N, 0.62; Found: C, 88.5; H, 10.9; N, 0.69.

**Preparation of CPdots.** The green-emitting CPdots from PQ in aqueous solution were prepared using the reprecipitation method. PQ was dissolved in THF to make a 1 mg/mL stock solution. One mL of the solution was quickly injected into Milli-Q water (12 mL) in a bath sonicator. The THF was removed by nitrogen stripping. The solution was filtered with a 0.45  $\mu\text{m}$  syringe cellulose acetate filter (Advantec). The CPdot dispersion remained clear and stable for 2 weeks without aggregation.

**Preparation of PVA–TEOS Solution.**<sup>69</sup> TEOS solution was prepared by dissolving TEOS in ethanol and deionized water with a molar ratio of 1.11:3:7 (TEOS:ethanol:water). After the dropwise addition of hydrochloric acid to reach a solution concentration of 0.1 M, the mixture was stirred at 60 °C for more than an hour. Afterward, aqueous PVA solution (7 wt %) was gradually added to the TEOS solution, and the mixture was thoroughly mixed with stirring at 60 °C for 1 h. Then, the mixture was cooled to room temperature and used for electrospinning.

**Electrospinning.** A power supply (Chungpa EMT Co., Ltd.; CPS-40K03, Seoul, Korea) was used to apply voltage to the electrospinning solution.<sup>38</sup> Electrospinning was carried out using a 10 mL syringe and a 21 gauge stainless steel capillary metal needle with a flat tip at an applied voltage of 20 kV. The positive electrode (NanoNC; ESR200R2, Seoul, Korea) of the power supply was attached to a collector wrapped in aluminum foil. The syringe pump was set to deliver the polymer solution at a feeding rate of 0.5 mL/h. The nanofibers were spun at a constant tip-to-collector distance of 10 cm. All processes were carried out under ambient conditions, and the thickness of the electrospun sheets was controlled by adjusting the spinning time.

**Amine Modification of PVA–Silica Nanofibers.**<sup>69</sup> The electrospun PVA–silica nanofibers were treated with APTES in toluene solution (2 wt %) for 1 h, and then baked at 100 °C for 30 min. The resultant amine-modified PVA–silica nanofibers were washed successively with toluene, a mixture of toluene and acetone, and acetone for 10 min each to remove the unreacted APTES.

**CPdots-Immobilized PVA–Silica Nanofibers.** The amine-modified PVA–silica nanofibers were immersed in aqueous CPdot solution for 1 h. Then, the nanofibers were washed with water three times. The DoF structure was stable even after washing for 1 h and centrifugation.

**Detection of Chemical Warfare Gas Simulants.** Chemical warfare gas detection was carried out with DoF with a size of 5 mm  $\times$  5 mm. The DoF was immersed in different ethanolic organophosphorous solutions (from  $6.0 \times 10^{-4}$  to  $1.8 \times 10^{-3}$  M) for 10 min and air-dried. The fluorescence spectral changes of the DoF in the presence of DCP, DMMP, TEP, and TBP were recorded.

## ■ ASSOCIATED CONTENT

### 📄 Supporting Information

Fluorescence images of PQ in chloroform solutions and DoF, DLS spectrum of CPdots, IR spectra, TG thermograms, XPS spectra of PVA and PVA–silica nanofibers, and SEM images. This material is available free of charge via the Internet at <http://pubs.acs.org>.

## ■ AUTHOR INFORMATION

### ✉ Corresponding Author

\*E-mail: [tslee@cnu.ac.kr](mailto:tslee@cnu.ac.kr).

### Notes

The authors declare no competing financial interest.

## ■ ACKNOWLEDGMENTS

Financial support from the National Research Foundation of Korea (NRF) funded by Korean government through the Basic Science Research Program (2012R1A2A2A01004979) is gratefully acknowledged.

## ■ REFERENCES

- (1) Friend, R. H.; Gymer, R. W.; Holmes, A. B.; Burroughes, J. H.; Marks, R. N.; Taliani, C.; Bradley, D. D. C.; Dos Santos, D. A.; Bredas, J. L.; Logdlund, M.; Salaneck, W. R. Electroluminescence in Conjugated Polymers. *Nature* **1999**, *397*, 121–128.
- (2) Baldo, M. A.; Thompson, M. E.; Forrest, S. R. High-Efficiency Fluorescent Organic Light-Emitting Devices Using a Phosphorescent Sensitizer. *Nature* **2000**, *403*, 750–753.
- (3) McQuade, D. T.; Pullen, A. E.; Swager, T. M. Conjugated Polymer-Based Chemical Sensors. *Chem. Rev.* **2000**, *100*, 2537–2574.
- (4) Achyuthan, K. E.; Bergstedt, T. S.; Chen, L.; Jones, R. M.; Kumaraswamy, S.; Kushon, S. A.; Lay, K. D.; Lu, L.; McBranch, D.; Mukundan, H.; Rininsland, F.; Shi, X.; Xia, W.; Whitten, D. G. Fluorescence Superquenching of Conjugated Polyelectrolytes: Applications for Biosensing and Drug Discovery. *J. Mater. Chem.* **2005**, *15*, 2648–2656.
- (5) Liu, M.; Kaur, P.; Waldeck, D. H.; Xue, C.; Liu, H. Fluorescence Quenching Mechanism of a Polyphenylene Polyelectrolyte with Other Macromolecules: Cytochrome c and Dendrimers. *Langmuir* **2005**, *21*, 1687–1690.
- (6) Kim, D.; Jang, G.; Kim, J.; Seo, S.; Park, W. H.; Lee, T. S. Cobalt Ion-Mediated Cysteine Detection With a Hyperbranched Conjugated Polyelectrolyte as a New Sensing Platform. *Macromol. Rapid Commun.* **2012**, *33*, 1510–1516.
- (7) Duan, R.; Ye, L.; Guo, X.; Huang, Y.; Wang, P.; Zhang, S.; Zhang, J.; Huo, L.; Hou, J. Application of Two-Dimensional Conjugated Benzo[1,2-b:4,5-b']dithiophene in Quinoxaline-Based Photovoltaic Polymers. *Macromolecules* **2012**, *45*, 3032–3038.
- (8) Du, X.; Qi, J.; Zhang, Z.; Ma, D.; Wang, Z. Y. Efficient Non-doped Near Infrared Organic Light-Emitting Devices Based on Fluorophores with Aggregation-Induced Emission Enhancement. *Chem. Mater.* **2012**, *24*, 2178–2185.
- (9) Jo, S.; Kim, D.; Son, S.-H.; Kim, Y.; Lee, T. S. Conjugated Poly(fluorene-quinoxaline) for Fluorescence Imaging and Chemical Detection of Nerve Agents with Its Paper-Based Strip. *ACS Appl. Mater. Interfaces* **2014**, *6*, 1330–1336.
- (10) Pecher, J.; Mecking, S. Nanoparticles of Conjugated Polymers. *Chem. Rev.* **2010**, *110*, 6260.
- (11) Tuncel, D.; Demir, H. V. Conjugated Polymer Nanoparticles. *Nanoscale* **2010**, *2*, 484–494.
- (12) Wu, C.; Chiu, D. T. Highly Fluorescent Semiconducting Polymer Dots for Biology and Medicine. *Angew. Chem., Int. Ed.* **2013**, *52*, 3086–3109.
- (13) Wu, C.; Bull, B.; Szymanski, C.; Christensen, K.; McNeill, J. Multicolor Conjugated Polymer Dots for Biological Fluorescence Imaging. *ACS Nano* **2008**, *2*, 2415–2423.



- (14) Fernando, L. P.; Kandel, P. K.; Yu, J.; McNeill, J.; Ackroyd, P. C.; Christensen, K. A. Mechanism of Cellular Uptake of Highly Fluorescent Conjugated Polymer Nanoparticles. *Biomacromolecules* **2010**, *11*, 2675–2682.
- (15) Vokatá, T.; Moon, J. H. Synthesis of Phenyleneethynylene-Doped Poly(p-phenylenebutadiynylene)s for Live Cell Imaging. *Macromolecules* **2013**, *46*, 1253.
- (16) Jin, Y.; Ye, F.; Wu, C.; Chan, Y.-H.; Chiu, D. T. Generation of Functionalized and Robust Semiconducting Polymer Dots with Polyelectrolytes. *Chem. Commun.* **2012**, *48*, 3161–3163.
- (17) Bu, J.; Watanabe, K.; Hayasaka, H.; Akagi, K. Photochemically Colour-Tuneable White Fluorescence Illuminants Consisting of Conjugated Polymer Nanospheres. *Nat. Commun.* **2014**, *5*, 3799.
- (18) Pu, K.; Li, K.; Shi, J.; Liu, B. Fluorescent Single-Molecular Core–Shell Nanospheres of Hyperbranched Conjugated Polyelectrolyte for Live-Cell Imaging. *Chem. Mater.* **2009**, *21*, 3816–3822.
- (19) Howes, P.; Green, M.; Levitt, J.; Suhling, K.; Hughes, M. Phospholipid Encapsulated Semiconducting Polymer Nanoparticles: Their Use in Cell Imaging and Protein Attachment. *J. Am. Chem. Soc.* **2010**, *132*, 3989–3996.
- (20) Noh, J.; Chae, B.-J.; Ku, B.-C.; Lee, T. S. Fabrication of a nanohybrid of conjugated polymer nanoparticles and graphene oxide for biosensing of trypsin. *J. Polym. Sci., Part A: Polym. Chem.* **2014**, *52*, 1898–1904.
- (21) Genin, E.; Gao, Z.; Varela, J. A.; Daniel, J.; Bsaibess, T.; Gosse, I.; Groc, L.; Cognet, L.; Blanchard-Desce, M. “Hyper-bright” Near-Infrared Emitting Fluorescent Organic Nanoparticles for Single Particle Tracking. *Adv. Mater.* **2014**, *26*, 2258–2261.
- (22) Li, K.; Zhan, R.; Feng, S.-S.; Liu, B. Conjugated Polymer Loaded Nanospheres with Surface Functionalization for Simultaneous Discrimination of Different Live Cancer Cells under Single Wavelength Excitation. *Anal. Chem.* **2011**, *83*, 2125–2132.
- (23) Shi, W.; Zeng, H.; Sahoo, Y.; Ohulchanskyy, T. Y.; Ding, Y.; Wang, Z. L.; Swihart, M.; Prasad, P. N. A General Approach to Binary and Ternary Hybrid Nanocrystals. *Nano Lett.* **2006**, *6*, 875–881.
- (24) Mokari, T. Synthesis and Characterization of Hybrid Nanostructures. *Nano Rev.* **2011**, *2*, 5983.
- (25) Katz, E.; Willner, I. Integrated Nanoparticle–Biomolecule Hybrid Systems: Synthesis, Properties, and Applications. *Angew. Chem., Int. Ed.* **2004**, *43*, 6042–6108.
- (26) Cheng, L.; Yang, K.; Li, Y.; Chen, J.; Wang, C.; Shao, M.; Lee, S. T.; Liu, Z. Facile Preparation of Multifunctional Upconversion Nanoprobes for Multimodal Imaging and Dual-Targeted Photothermal Therapy. *Angew. Chem., Int. Ed.* **2011**, *50*, 7385–7390.
- (27) Nair, L. V.; Nagaota, Y.; Maekawa, T.; Sakthikumar, D.; Jayasree, R. S. Quantum Dot Tailored to Single Wall Carbon Nanotubes: A Multifunctional Hybrid Nanoconstruct for Cellular Imaging and Targeted Photothermal Therapy. *Small* **2014**, *10*, 2771–2775.
- (28) Xia, Y.; Yang, P.; Sun, Y.; Wu, Y.; Mayers, B.; Gate, B.; Yin, Y.; Kim, F.; Yan, H. One-Dimensional Nanostructures: Synthesis, Characterization, and Applications. *Adv. Mater.* **2003**, *15*, 353–389.
- (29) Zheng, H.; Li, Y.; Liu, H.; Yin, X.; Li, Y. Construction of Heterostructure Materials Toward Functionality. *Chem. Soc. Rev.* **2011**, *40*, 4506–4524.
- (30) Geng, J.; Liu, J.; Liang, J.; Shi, H.; Liu, B. A General Approach to Prepare Conjugated Polymer Dot Embedded Silica Nanoparticles with a SiO<sub>2</sub>@CP@SiO<sub>2</sub> Structure for Targeted HER2-Positive Cellular Imaging. *Nanoscale* **2013**, *5*, 8593–8601.
- (31) Yang, Y.; Wang, H.; Su, K.; Long, Y.; Peng, Z.; Li, N.; Liu, F. Facile and Sensitive Fluorescent Sensor Using Electrospun Nanofibrous Film for Nitroaromatic Explosive Detection. *J. Mater. Chem.* **2011**, *21*, 11895–11900.
- (32) He, X.; Tan, L.; Wu, X.; Yan, C.; Chen, D.; Meng, X.; Tang, F. Electrospun Quantum Dots/Polymer Composite Porous Fibers for Turn-On Fluorescent Detection of Lactate Dehydrogenase. *J. Mater. Chem.* **2012**, *22*, 18471–18478.
- (33) Wu, Y.-N.; Zhang, B.; Li, F.; Zhu, W.; Xu, D.; Hannam, P.; Li, G. Electrospun Fibrous Mats as a Skeleton for Fabricating Hierarchically Structured Materials as Sorbents for Cu<sup>2+</sup>. *J. Mater. Chem.* **2012**, *22*, 5089–5097.
- (34) Tao, S.; Li, G.; Yin, J. Fluorescent Nanofibrous Membranes for Trace Detection of TNT Vapor. *J. Mater. Chem.* **2007**, *17*, 2730–2736.
- (35) Lee, J.; Balakrishnan, S.; Cho, J.; Jeon, S.-H.; Kim, J.-M. Detection of Adulterated Gasoline Using Colorimetric Organic Microfibers. *J. Mater. Chem.* **2011**, *21*, 2648–2655.
- (36) Crespy, D.; Friedemann, K.; Popa, A.-M. Colloid-Electrospinning: Fabrication of Multicompartment Nanofibers by the Electrospinning of Organic or/and Inorganic Dispersions and Emulsions. *Macromol. Rapid Commun.* **2012**, *33*, 1978–1995.
- (37) Müller, K.; Quinn, J. F.; Johnston, A. P. R.; Becker, M.; Greiner, A.; Caruso, F. Polyelectrolyte Functionalization of Electrospun Fibers. *Chem. Mater.* **2006**, *18*, 2397–2403.
- (38) Kim, J.; Noh, J.; Jo, S.; Park, K. E.; Park, W. H.; Lee, T. S. Simple Technique for Spatially Separated Nanofibers/Nanobeads by Multinozzle Electrospinning toward White-Light Emission. *ACS Appl. Mater. Interfaces* **2013**, *5*, 6038–6044.
- (39) Li, M.; Zhang, J.; Zhang, H.; Liu, Y.; Wang, C.; Xu, X.; Tang, Y.; Yang, B. Electrospinning: A Facile Method to Disperse Fluorescent Quantum Dots in Nanofibers without Förster Resonance Energy Transfer. *Adv. Funct. Mater.* **2007**, *17*, 3650–3656.
- (40) Atchison, J. S.; Schauer, C. L. Fabrication and Characterization of Electrospun Semiconductor Nanoparticle–Polyelectrolyte Ultra-Fine Fiber Composites for Sensing Applications. *Sensors* **2011**, *11*, 10372–10387.
- (41) Madhugiri, S.; Dalton, A.; Gutierrez, J.; Ferraris, J. P.; Balkus, K. J., Jr. Electrospun MEH-PPV/SBA-15 Composite Nanofibers Using a Dual Syringe Method. *J. Am. Chem. Soc.* **2003**, *125*, 14531–14538.
- (42) Acosta, C.; Pérez–Esteve, E.; Fuenmayor, C. A.; Benedetti, S.; Cosio, M. S.; Soto, J.; Sancenón, F.; Mannino, S.; Barat, J.; Marcos, M. D.; Martínez-Mañez, R. Polymer Composites Containing Gated Mesoporous Materials for On-Command Controlled Release. *ACS Appl. Mater. Interfaces* **2014**, *6*, 6453–6460.
- (43) Kanjanapongkul, K.; Wongsasulak, S.; Yoovidhya, T. Investigation and Prevention of Clogging during Electrospinning of Zein Solution. *J. Appl. Polym. Sci.* **2010**, *118*, 1821–1829.
- (44) Jeong, J. S.; Jeon, S. Y.; Lee, T. Y.; Park, J. H.; Shin, J. S.; Alegaonkar, P. S.; Berdinsky, A. S.; Yoo, J. B. Fabrication of MWNTs/Nylon Conductive Composite Nanofibers by Electrospinning. *Diamond Relat. Mater.* **2006**, *15*, 1839–1843.
- (45) Dong, H.; Wang, D.; Sun, G.; Hinstroza, J. P. Assembly of Metal Nanoparticles on Electrospun Nylon 6 Nanofibers by Control of Interfacial Hydrogen-Bonding Interactions. *Chem. Mater.* **2008**, *20*, 6627–6632.
- (46) Son, H. Y.; Ryu, J. H.; Lee, H.; Nam, Y. S. Bioinspired Templating Synthesis of Metal-Polymer Hybrid Nanostructures within 3D Electrospun Nanofibers. *ACS Appl. Mater. Interfaces* **2013**, *5*, 6381–6390.
- (47) Marrs, T. C. Organophosphate Poisoning. *Pharmacol. Ther.* **1993**, *58*, 51–66.
- (48) Kim, K.; Tsay, O. G.; Atwood, D. A.; Churchill, D. G. Destruction and Detection of Chemical Warfare Agents. *Chem. Rev.* **2011**, *111*, 5345–5403.
- (49) Royo, S.; Martínez–Mañez, R.; Sancenón, F.; Costero, A. M.; Parra, M.; Gil, S. Chromogenic and Fluorogenic Reagents for Chemical Warfare Nerve Agents’ Detection. *Chem. Commun.* **2007**, *46*, 4839–4847.
- (50) Kim, T. H.; Kim, D. G.; Lee, M.; Lee, T. S. Synthesis of Reversible Fluorescent Organogel Containing 2-(2′-Hydroxyphenyl)-benzoxazole: Fluorescence Enhancement upon Gelation and Detecting Property for Nerve Gas Simulant. *Tetrahedron* **2010**, *66*, 1667.
- (51) Kim, H. J.; Lee, J. H.; Lee, H.; Lee, J. H.; Lee, J. H.; Jung, J. H.; Kim, J. S. A Mesoporous, Silica-Immobilized-Nanoparticle Colorimetric Chemosensor for the Detection of Nerve Agents. *Adv. Funct. Mater.* **2011**, *21*, 4035–4040.
- (52) Wu, W.; Dong, J.; Wang, X.; Li, J.; Sui, S.; Chen, G.; Liu, J.; Zhang, M. Fluorogenic and Chromogenic Probe for Rapid Detection of a Nerve Agent Simulant DCP. *Analyst* **2012**, *137*, 3224–3226.

- (53) Zhang, S. W.; Swager, T. M. Fluorescent Detection of Chemical Warfare Agents: Functional Group Specific Ratiometric Chemosensors. *J. Am. Chem. Soc.* **2003**, *125*, 3420–3421.
- (54) Pangen, D.; Nesterov, E. E. Higher Energy Gap” Control in Fluorescent Conjugated Polymers: Turn-On Amplified Detection of Organophosphorous Agents. *Macromolecules* **2013**, *46*, 7266–7273.
- (55) Kim, H. J.; Lee, J. H.; Lee, M.; Lee, T. S. Optical Switching and Anion-Induced Chromogenic Application in Conjugated Polyazomethine Derivatives. *React. Funct. Polym.* **2008**, *68*, 1696–1703.
- (56) Kim, Y. H.; Shin, D. C.; Kim, S.-H.; Ko, C.-H.; Yu, H.-S.; Chae, Y.-S.; Kwon, S. K. Novel Blue Emitting Material with High Color Purity. *Adv. Mater.* **2001**, *13*, 1690–1693.
- (57) Satrijo, A.; Swager, T. M. Anthryl-Doped Conjugated Polyelectrolytes as Aggregation-Based Sensors for Nonquenching Multicationic Analytes. *J. Am. Chem. Soc.* **2007**, *129*, 16020–16028.
- (58) Satrijo, A. S.; Kooi, E.; Swager, T. M. Enhanced Luminescence from Emissive Defects in Aggregated Conjugated Polymers. *Macromolecules* **2007**, *40*, 8833–8841.
- (59) Kwon, N. Y.; Kim, D. G.; Son, J. H.; Jang, G.; Lee, J. H.; Lee, T. S. Simultaneous Detection and Removal of Mercury Ions in Aqueous Solution with Fluorescent Conjugated Polymer-Based Sensor Ensemble. *Macromol. Rapid Commun.* **2011**, *32*, 1061–1065.
- (60) Kwon, N. Y.; Jang, G.; Kim, D.; Kim, J.; Lee, T. S. Oligonucleotide-Mediated Aggregation of a Cationic Conjugated Polymer for Fluorescent Detection of Mercury Ions in an Aqueous Medium. *J. Polym. Sci., Part A: Polym. Chem.* **2013**, *51*, 2393–2400.
- (61) Kwon, N. Y.; Kim, D.; Jang, G.; Lee, J. H.; So, J.-H.; Kim, C.-H.; Kim, T. H.; Lee, T. S. Highly Selective Cysteine Detection and Bioimaging in Zebrafish through Emission Color Change of Water-Soluble Conjugated Polymer-Based Assay Complex. *ACS Appl. Mater. Interfaces* **2012**, *4*, 1429–1433.
- (62) Lee, J. H.; Kim, D. G.; Kwon, N. Y.; Jang, G.; Son, J. H.; Lee, M. J.; Cho, H.; Kweon, H.; Lee, T. S. Protein-Induced Aggregation of Fluorescent Conjugated Polyelectrolytes with Sulfonate Groups: Synthesis and Its Sensing Application. *J. Polym. Sci., Part A: Polym. Chem.* **2011**, *49*, 138–146.
- (63) Liu, S.; Zhang, Z.; Zhang, H.; Zhang, Y.; Wei, S.; Ren, L.; Wang, C.; He, Y.; Li, F.; Xiao, F. S. Phase Separation of Organic/Inorganic Hybrids Induced by Calcination: A Novel Route for Synthesizing Mesoporous Silica and Carbon Materials. *J. Colloid Interface Sci.* **2010**, *345*, 257–261.
- (64) Noh, J.; Kim, D.; Jang, G.; Kim, J.; Heo, M. B.; Lee, N.-E.; Kim, C.-Y.; Lee, E.; Kim, Y.-J.; Lim, Y. T.; Lee, T. S. Fabrication, Biofunctionalization, and Simultaneous Multicolor Emission of Hybrid “Dots-on-Spheres” Structures for Specific Targeted Imaging of Cancer Cells. *RSC Adv.* **2014**, *4*, 41378–41386.
- (65) Thomas, J. K. Physical Aspects of Radiation-Induced Processes on SiO<sub>2</sub>,  $\gamma$ -Al<sub>2</sub>O<sub>3</sub>, Zeolites, and Clays. *Chem. Rev.* **2005**, *105*, 1683–1734.
- (66) Xu, X. Z.; Han, Y.; Li, D.; Ding, H.; Wang, Y.; Xiao, F.-S. Improved Structural Order, Stability, and Anion-Exchange Capacity of Cation-Mediated Bridged Hybrid Mesoscopic Materials by Using Chelating Ligands. *Chem. Mater.* **2004**, *16*, 3507–3512.
- (67) Xie, Z.; Wang, F.; Liu, C. Organic–Inorganic Hybrid Functional Carbon Dot Gel Glasses. *Adv. Mater.* **2012**, *24*, 1716–1721.
- (68) Kim, T. H.; Kim, H. J.; Kwak, C. G.; Park, W. H.; Lee, T. S. Aromatic Oxadiazole-Based Conjugated Polymers with Excited-State Intramolecular Proton Transfer: Their Synthesis and Sensing Ability for Explosive Nitroaromatic Compounds. *J. Polym. Sci., Part A: Polym. Chem.* **2006**, *44*, 2059–2068.
- (69) Nakane, K.; Yamashita, T.; Iwakura, K.; Suzuki, F. Properties and Structure of Poly(Vinyl Alcohol)/Silica Composites. *J. Appl. Polym. Sci.* **1999**, *74*, 133–138.